JGR Atmospheres

RESEARCH ARTICLE
10.1029/2020JD032914

Key Points:
- Probabilistic projections of hydrological drought characteristics are developed at a river basin scale
- Hydrological droughts are expected to occur more frequently by the end of the 21st century
- The number of dry-wet abrupt alternation event is projected to increase in a changing climate

Supporting Information:
- Supporting Information S1

Correspondence to:
S. Wang,
shuo.s.wang@polyu.edu.hk

Citation:
Chen, H., Wang, S., Wang, Y., & Zhu, J. (2020). Probabilistic projections of hydrological droughts through convection-permitting climate simulations and multimodel hydrological predictions. *Journal of Geophysical Research: Atmospheres*, *125*, e2020JD032914. https://doi.org/10.1029/2020JD032914

Received 12 APR 2020
Accepted 18 JUL 2020
Accepted article online 21 JUL 2020

Author Contributions:
Conceptualization: S. Wang
Data curation: S. Wang, Y. Wang
Formal analysis: H. Chen
Funding acquisition: S. Wang
Investigation: S. Wang
Methodology: H. Chen, S. Wang
Project administration: S. Wang
Resources: S. Wang
Supervision: S. Wang
Validation: H. Chen, Y. Wang, J. Zhu
Visualization: H. Chen, Y. Wang
Writing - original draft: H. Chen
Writing – review & editing: S. Wang, J. Zhu

Probabilistic Projections of Hydrological Droughts Through Convection-Permitting Climate Simulations and Multimodel Hydrological Predictions

H. Chen[1], S. Wang[1,2], Y. Wang[3], and J. Zhu[1]

[1]Department of Land Surveying and Geo-Informatics, The Hong Kong Polytechnic University, Hong Kong, China, [2]Shenzhen Research Institute, The Hong Kong Polytechnic University, Shenzhen, China, [3]Department of Geosciences, Texas Tech University, Lubbock, TX, USA

Abstract The reliable projection of future changes in hydrological drought characteristics plays a crucial role in providing meaningful insights into agricultural development and water resources planning under climate change. In this study, we develop probabilistic projections of hydrological drought characteristics through a convection-permitting climate simulation and a multimodel hydrological prediction for two major river basins in South Texas of the United States. The probabilistic hydrological drought projection depicts the future evolution of spatiotemporal characteristics of droughts under best- and worst-case scenarios. Our findings reveal that there is a considerable variation in hydrological drought regimes near the urban area in South Texas. And the prolonged severe drought events are expected to be punctuated by the increasing extreme precipitation in a changing climate. This could lead to an increasing number of the dry-wet abrupt alternation events. Moreover, hydrological droughts are projected to occur more frequently for the fall season in the Guadalupe River Basin and for the winter season in the Blanco River Basin, advancing our understanding of future changes in seasonal characteristics of hydrological droughts at a river basin scale.

1. Introduction

Drought is a disastrous natural phenomenon as a result of the precipitation deficit in a particular region (Schlaepfer et al., 2017), which has far-reaching effects on society and the environment, such as the depletion of water supplies, severe wildfires, and the reduction of crop production (Li et al., 2019; Naumann et al., 2018). A variety of hydroclimatic variables can be used to detect and assess drought hazards, including precipitation, streamflow, soil moisture, snowmelt, and potential evapotranspiration (PET) (McKee et al., 1993). Based on these variables and their combinations, droughts can be categorized into meteorological, hydrological, agricultural, and socioeconomic droughts (Oguntunde et al., 2017; Zargar et al., 2011; Q. Zhang & Zhang, 2016).

Different types of droughts are correlated with each other as they originate from a deficiency of precipitation. The meteorological and agricultural droughts have been widely studied over the past decade. By contrast, the hydrological drought has been attracting increasing attention from climatologists and hydrologists in recent years. The hydrological drought has a widespread impact on agricultural production and socioeconomic development due to the significant reduction in the water supply, thereby resulting in a series of chain effects such as the decrease in agricultural irrigation, the deterioration in water quality, and the reduction in hydropower generation (Mishra & Singh, 2010; Tabari et al., 2013; Zhu et al., 2019). It is thus necessary to examine changes of hydrological drought characteristics in a changing climate, which plays a crucial role in reducing potential risks and damages caused by drought hazards. To understand the hydrological drought evolution under climate change, streamflow is the key variable of assessing climate change impacts on water availability in the hydrological system (Carvalho & Wang, 2019; Modarres, 2007; Tabari et al., 2013; Vicente-Serrano et al., 2011; Yu et al., 2015).

A variety of drought indicators have been developed for assessing the hydrological drought over the past decades (Zargar et al., 2011), including Palmer Hydrological Drought Index (PHDI) (Karl, 1986), Surface Water Supply Index (SWSI) (Shafer, 1982), Reconnaissance Drought Index (RDI) (Tsakiris et al., 2007), Standardized Runoff Index (SRI) (Shukla & Wood, 2008), Streamflow Drought Index (SDI) (Nalbantis &

Tsakiris, 2009), Standardized Streamflow Index (SSI) (Vicente-Serrano et al., 2011), and Standardized Supply-demand Water Index (SSDI) (Yuan et al., 2017). All these indices were mainly used to analyze historical hydrological drought regimes based on the observations from meteorological and hydrological stations. Although it is important to understand historical drought events, predicting future changes in climate-induced droughts is useful for policymakers and stakeholders to develop sound climate change mitigation and adaptation strategies. It can be expected that the future hydrological drought would become severer due to the changing climate and the depletion of water resources caused by population explosion (Pereira et al., 2018; Q. Zhang & Zhang, 2016; Zou et al., 2018).

In recent years, many studies have been devoted to the prediction of the future hydrological drought caused by the human-induced climate change (Liu et al., 2012; Oguntunde et al., 2018; Yu et al., 2015; Yuan et al., 2017; B. Zhang et al., 2019). For example, Z. L. Wang, Zhong, et al. (2018) evaluated future droughts in the Pearl River Basin using the Palmer Drought Severity Index (PDSI) based on the climate projections of General Circulation Models (GCMs) from Phase 5 of the Coupled Model Inter-comparison Project (CMIP5) under different Representative Concentration Pathways (RCPs) scenarios. Vu et al. (2017) examined future drought conditions in the Vu Gia-Thu River basin using the Standardized Precipitation Index (SPI) and SRI based on the climate variables projected from regional climate models. Oguntunde et al. (2017) examined the features of future droughts in the Volta River Basin using the Standardized Precipitation Evapotranspiration Index (SPEI), SPI, and SRI based on the climate outputs of eight GCMs. Previous studies of climate-induced hydrological droughts were mainly based on the coarse-resolution climate model simulations, which might result in unreliable drought assessment due to the inability of models to represent the temporal and spatial heterogeneities in precipitation with complex geographical features (e.g., mountains, coastlines, and land covers). Furthermore, the small-scale physical processes such as cloud formation and convective precipitation are approximated by parameterization schemes in climate modeling, which is considered as a major source of model errors and uncertainties in climate simulations (Prein et al., 2015). This can result in unreliable assessment of hydrological droughts at a river basin scale.

To improve the projections of future changes in precipitation and hydrological drought characteristics, the convection-permitting climate simulations can be performed to explicitly resolve the small-scale climate dynamics without the use of convective parameterization (Prein et al., 2015). The convection-permitting climate modeling with the horizontal grid spacing $\leq$4 km is recognized as a powerful means to provide more realistic representation of convection and can be used to simulate the possibility of localized high-impact rainfall not resolved by coarser-resolution climate models (Kendon et al., 2017). Thus, the convection-permitting climate modeling can be used to well simulate the spatial and temporal variability of precipitation, which is the most important climate variable for assessing all types of droughts (Chen et al., 2020; Wang, Huang, et al., 2017). In addition, uncertainties are inevitable in hydrological drought assessment, mainly including model structural and parameter uncertainties (Samaniego et al., 2013). It is thus desired to address both model structural and parameter uncertainties in order to improve the reliability and robustness of hydrological drought assessment.

The objective of this study is to develop probabilistic projections of hydrological drought characteristics by addressing both model structural and parameter uncertainties through the convection-permitting climate simulations. The Climate Forecast System Reanalysis (CFSR) reanalysis data set will be dynamically downscaled into the high-resolution climate information using the Weather Research and Forecasting (WRF) model. The projected climatic variables will then be used to drive two hydrological models to predict future changes in runoff characteristics for two major river basins in South Texas. A weighted-average aggregation method will be used to address model structural uncertainty and the Markov chain Monte Carlo (MCMC) simulation will be performed to tackle model parameter uncertainty inherent in hydrological predictions, leading to probabilistic projections of hydrological droughts in a changing climate.

This paper is organized as follows. In section 2, data sets, models, the experiment design, and drought indices used in this study will be described. In section 3, the convection-permitting WRF simulation and the probabilistic hydrological prediction will be verified against observations. In addition, future changes in hydrological droughts response to climate change will be analyzed and uncertainties in hydrological drought projections will also be assessed. In section 4, the primary novelty of this work and major findings will be highlighted.

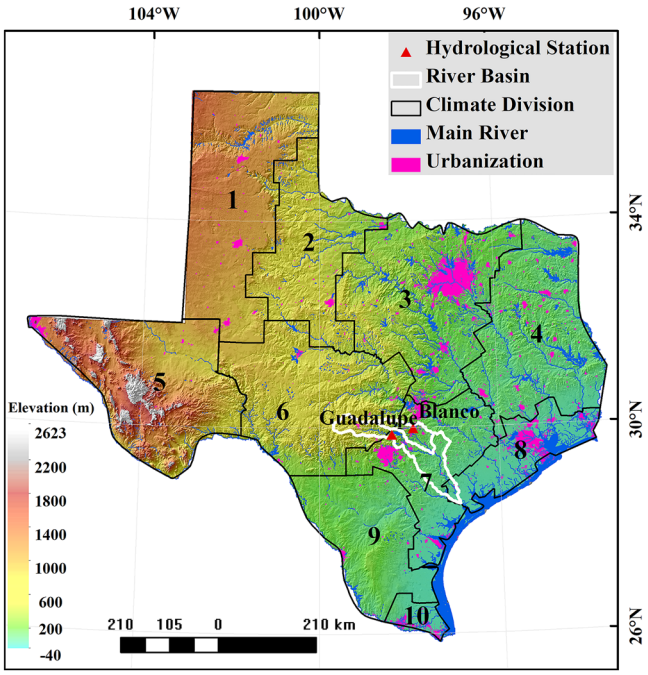

Figure 1. The WRF model domain and topography over 10 climate divisions in Texas. Red triangles represent the location of hydrological station. Two major river basins of South Texas and urban areas are highlighted in white and pink, respectively.

2. Data Sets, Models, and Drought Indices

2.1. Data Sources and Study Region

In this study, the observation used to validate the WRF model is the Parameter-elevation Regressions on Independent Slopes Model (PRISM) data set (with a 4 km × 4 km spatial resolution) developed by the Oregon State University's Climate Group (Daly et al., 2008). The PRISM interpolates nearly 13,000 surface stations for precipitation by using a "terrain-aware" technique. These station data are mainly obtained from the Snowpack Telemetry network and the National Weather Service Cooperative Observer Program (COOP) gauge network. The precipitation of PRISM has been commonly used as a reference in many climate studies (Liu et al., 2017; Silverman et al., 2013; Wang, Ancell, et al., 2018; Wang, Geerts, et al., 2018). The PRISM data from 1981 to 1995 were bilinearly interpolated to the WRF grids for spatial comparison between simulated and observed climate variables.

To carry out the climate projection using the convection-permitting WRF model, a perturbed ensemble mean climate change signal was created from a total of 15 CMIP5 GCMs (see Table S1 in the supporting information) based on the assessment of model performance in simulating current climate over North America (Liu et al., 2017).

Model Parameter Estimation Experiment (MOPEX) is an international project aimed to develop techniques for a priori estimation of parameters in hydrologic models and in land surface parameterization schemes of atmospheric models. The MOPEX data set contains a large number of high-quality historical hydrometeorological data and land surface characteristics data for a wide range of river basins around the world (Duan et al., 2006). Thus, the MOPEX data sets were used to conduct hydrological simulations for two major river basins in South Texas, including Guadalupe River Basin (GRB) and Blanco River Basin (BRB), over the period from January 1981 to December 1995. The data of the first year were used to spin up the model in order to reach an equilibrium state for hydrological simulations. The remaining 15-year data were used to simulate daily streamflow in the two river basins. The U.S. Geological Survey (USGS) gauging station data were also collected to calibrate and validate the hydrological models. Specifically, both the HYMOD and SWAT models were calibrated against the observed streamflow for the period from 1981 to 1990 and then were validated for the 5-year period from 1991 to 1995.

The BRB and the GRB form the northern and northwestern headwaters of the larger Guadalupe river system, respectively. The BRB is characterized by karst landscape that consists of limestone and thin soils surface (<1 m), while the GRB varies from the steep, limestone hill that is prone to flash flooding. Climate in Guadalupe river system is considered as subtropical humid with short mild winters and hot summers. The region is prone to suffer from frequent droughts; however, later spring and early fall are the wettest period for the passage of continental fronts, which bring short-duration high-intensity events. Such climatic features are prone to suffer from hydrological extremes (droughts and floods), it is thus expected to project future changes of hydrological drought characteristics in a changing climate.

2.2. Convection-Permitting Climate Modeling

In this study, the region of Texas is divided into 10 climate divisions according to the U.S. National Climatic Data Center (NCDC), as shown in Figure 1. The convection-permitting WRF model was used to simulate regional climate change over Texas. The computational domain has 380 × 350 horizontal grid points that cover a total area of 1,520 km × 1,400 km and 51 vertical levels topped at 50 hPa using a single-domain framework. The resolution of each grid box is 4 km × 4 km, which is fine enough to explicitly resolve the deep convection instead of parameterizing the convection process (Liu et al., 2011). The temporal resolution of model outputs is 6-hr intervals. The National Centers for Environmental Prediction (NCEP) Climate Forecast System Reanalysis (CFSR) data set with spatial resolution of 38 km was utilized as initial and

lateral boundary conditions to drive the WRF model. The historical WRF simulation is forced by the 6-hr CFSR with spatial resolution of 38 km for the period of 1981–1995. For the experimental design, the WRF model was configured with the Yongsei University planetary boundary layer scheme (Hong & Pan, 1996), the rapid radiative transfer model shortwave and longwave radiation scheme (Iacono et al., 2008), the Thompson cloud microphysics scheme (Thompson et al., 2008), the Noah-MP land surface scheme (Niu et al., 2011; Yang et al., 2011), and the revised Monin-Obukhov surface layer scheme (Jiménez et al., 2012). This model configuration was selected based on 3 years of the WRF simulations with optimal model performance for the study domain (Wang, Geerts, et al., 2018).

To carry out the future climate projection over a period of 15 years from 2085 to 2099, the Pseudo-Global Warming (PGW) approach was used to generate a perturbed climate change signal for producing future climate information. As shown in Equation 1, the future WRF simulation is forced by the CFSR with a climate perturbation for the future period of 2085–2099. The CFSR reanalysis data set is perturbed every 6 hr by the derived climate change signal to provide the WRF model with initial and boundary conditions for future climate projections under the RCP8.5 climate scenario. The climate perturbation is calculated by the 15-GCM ensemble-mean monthly change between a future 30-year monthly ensemble mean (2071–2100) and a historical 30-year monthly ensemble mean (1975–2005) (Rasmussen et al., 2017):

$$\mathrm{WRFinput}(2085\text{–}2099) = \mathrm{CFSR}_{2085\text{–}2099} + (\mathrm{CMIP52071\text{–}2100} - \mathrm{CMIP51976\text{–}2005}). \quad (1)$$

The perturbed climate change signal includes land surface temperature, geopotential height, humidity, horizontal wind, sea surface temperature, sea level pressure, and soil temperature (Liu et al., 2017; Rasmussen et al., 2017).

According to Deser et al. (2012) and Liu et al. (2017), the climate change signal from a single GCM may not be representative due to the large range of climate sensitivity (to greenhouse gas forcing) among current GCMs. Thus, the climate change signal was created in this study from a multi-GCM ensemble to improve the single-model-run method, which enabled us to exploit the large range of internal variability and climate sensitivity of GCMs. Nevertheless, a limitation of the PGW approach is the assumption that the year-to-year and short-term variations in the present climate are the same in the future (Wakazuki & Rasmussen, 2015).

2.3. Hydrological Model Structure and Parameter Estimation

To assess climate change impacts on hydrological characteristics, a conceptual model (HYMOD) and a physically based model (SWAT) were used to predict daily streamflow in two major river basins over South Texas based on the projected climate variables. The HYMOD and SWAT were combined into a general framework using a weighted-average aggregation method in order to address the model structural uncertainty. In addition, the PET was calculated using the FAO-Penman-Monteith equation due to its high accuracy of assessment at different time scales (Allen et al., 1998; Zotarelli et al., 2010). According to the equation, the PET can be estimated based on the air temperature, relative humidity, wind speed, and solar radiation simulated by the WRF model.

2.3.1. The HYMOD Model

The HYMOD has been widely used for uncertainty assessment of hydrological model parameters and predictions, and it has been applied to predict streamflow in various basins around the world (Abera et al., 2017; Herman et al., 2013; Roy et al., 2017; Wang & Wang, 2019). This model consists of a soil moisture accounting module and a routing module. The soil moisture accounting module is based on a probability-distributed soil function of soil moisture capacity module, as shown below (Moore, 1985):

$$\mathrm{F(C)}=1-\left(1-\frac{C}{C_{max}}\right)^{b_{exp}} \quad 0 \le \mathrm{C} \le C_{max}, \quad (2)$$

where F(C) represents the cumulative probability of a given water storage capacity (C). C_{max} stands for the maximum storage capacity of soil moisture, and b_{exp} is the shape factor that represents the degree of spatial variability of the soil moisture storage capacity. The routing module includes three quick flow tanks representing the surface flow and a single slow flow tank representing the subsurface flow. When the soil moisture capacity is exceeded, excess rainfall is divided into quick and slow flow tanks by a partitioning factor β. Streamflow is the addition of the outputs from quick and slow flow tanks. In this study, all

model parameters (C_{max}, b_{exp}, β, R_q, and R_s) were initially given with an uncertainty range (see Table S2) and then were calibrated against observations using the MCMC algorithm.

By using the MCMC algorithm within a Bayesian framework, the posterior distributions of hydrological model parameters were inferred by recursively updating information in the prior parameter distributions when new observations become available, as shown below:

$$\mathrm{p}(\theta|\tilde{\mathrm{Y}}) = \frac{p(\theta)p(\tilde{Y}|\theta)}{p(\tilde{Y})}, \tag{3}$$

$$\mathrm{p}(\theta|\tilde{\mathrm{Y}}) \propto p(\theta)L(\theta|\tilde{Y}), \tag{4}$$

where θ represents model parameters, $\tilde{\mathrm{Y}}$ represents observations, and p(θ) and p($\theta|\tilde{\mathrm{Y}}$) denote prior and posterior distributions of model parameters, respectively. As ($\tilde{\mathrm{Y}}$) can be treated as a normalization constant, Equation 3 can be simplified and transformed into Equation 4. In Equation 4, ($\theta|\tilde{\mathrm{Y}}$) represents the likelihood function that quantifies the probability of the observation data generated by a parameter set. Considering the difference between model simulations and observations based on the assumption that the error residuals are homoscedastic, uncorrelated, and Gaussian-distributed with mean zero (Sorooshian & Dracup, 1980), the likelihood function can be formulated as follows:

$$L(\theta|\tilde{\mathrm{Y}}) = \prod_{t=1}^{n} \frac{1}{\sqrt{2\pi\tilde{\sigma}^2}} exp\left\{-\frac{1}{2}\tilde{\sigma}^{-2}[\tilde{y_t} - y_t(\theta)]^2\right\}, \tag{5}$$

where $\tilde{\sigma}$ donates the standard deviation (SD) of the measurement error of observations, $\tilde{y_t}$ represents the observation at time t, and $y_t(\theta)$ is the model parameter θ given at time t. For algebraic simplicity and numerical stability (Sadegh et al., 2017), Equation 5 can be transformed into

$$L(\theta|\tilde{\mathrm{Y}}) = -\frac{n}{2}\ln(2\pi) - \frac{n}{2}\ln\tilde{\sigma}^2 - \frac{1}{2}\tilde{\sigma}^{-2}\sum_{t=1}^{n}[\tilde{y_t} - y_t(\theta)]^2. \tag{6}$$

When the prior distributions of model parameters are determined, the posterior parameter distributions can be derived through the MCMC simulation.

The Differential Evolution Adaptive Metropolis (DREAM) algorithm was adopted to implement the MCMC simulation. The algorithm was proposed by Vrugt et al. (2008) to run multiple Markov chains in parallel at the same time. For each Markov chain, it constructs a random walk with an acceptance/rejection rule to converge into a stationary distribution (Andrieu & Thoms, 2008). The random walk operates using the Metropolis algorithm introduced by Metropolis et al. (1953). The simulation runs constantly until the Markov chain converges into the stationary distribution with a posterior probability density function (PDF). The multichain $\widehat{R}$ diagnostic can then be used to determine the convergence of the DREAM algorithm (Gelman & Rubin, 1992). When the $\widehat{R}$-statistic drops below a value of 1.2, the convergence of the posterior distribution is achieved for model parameters (Vrugt, 2016).

2.3.2. The SWAT Model

The SWAT model (Gassman et al., 2007) is a physically based and continuous watershed simulation model, which is capable of simulating a high level of spatial details, and thus, it has been widely used for hydrological assessment. The SWAT model uses a basin discretization that divides the study area into several subbasins and Hydrological Response Units (HRUs), and subbasins have unique land use, soil, and slope categories (Neitsch et al., 2011; Rodrigues et al., 2015). Each HRU conducts a simulation of hydrological processes, and the output water fluxes are routed to the watershed to generate the total discharge values. The model simulates the hydrological processes at each HRU where water balance calculations are made (Neitsch et al., 2011). In this study, the SWAT model parameters were estimated with uncertainty ranges using the SWAT CUP software with the Sequential Uncertainty Fitting (SUFI-2) (Abbaspour et al., 2015), as shown in Table S3.

2.3.3. Hybrid Modeling (HYMOD-SWAT)

Both the HYMOD and SWAT models were used to simulate streamflow in the two major river basins for the 15-year period of 1981–1995, with a 1-year (1980) warm-up period. The calibration period was selected from

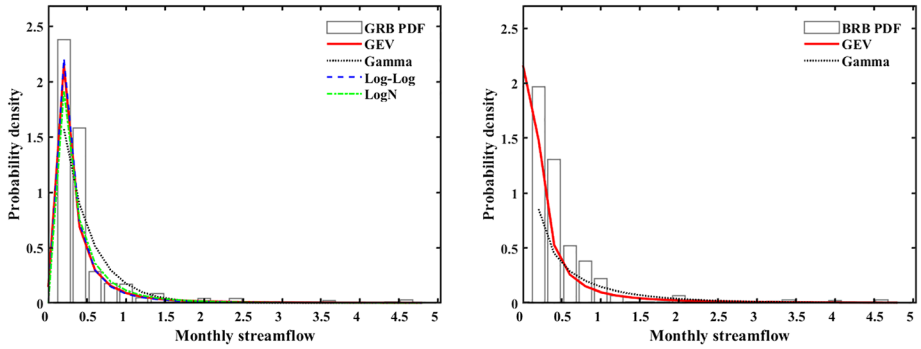

Figure 2. Comparison of different types of probability distributions that best fit monthly streamflow observations for Guadalupe River Basin (GRB) and Blanco River Basin (BRB).

1981 to 1990, and the validation period was from 1991 to 1995. The HYMOD and SWAT models were combined into a general framework using a weighted-average aggregation method (Rodrigues et al., 2015; Wilby & Harris, 2006). The weights were calculated in proportion to model performance based on the adjusted correlation coefficients (CORs), which were computed for the calibration period (1981–1990), and then the weights were applied for the validation period (1991–1995) and the forecast period (2085–2099) by

$$R_{adj} = \sqrt{1 - \frac{(1 - r^2)(n - 1)}{n - 2}}, \tag{7}$$

where R_{adj} is the adjusted COR, r is the linear COR, and n is the sample element. In this study, the linear COR was calculated based on the best model simulation with the minimum root mean square error (RMSE) and observation. As for BRB, R_{adj} of HYMOD = 0.82, and R_{adj} of SWAT = 0.80. As for GRB, R_{adj} of HYMOD = 0.84, and R_{adj} of SWAT = 0.80.

2.4. Standardized Runoff Index

To examine the climate change impacts on hydrological droughts, SRI was applied based on the monthly runoff in a given river basin (Shukla & Wood, 2008). SRI is recognized as a powerful indicator used to assess hydrological droughts while considering the effects of natural characteristics in different regions (Dehghani et al., 2014; Mishra & Singh, 2010; Oguntunde et al., 2017; Vu et al., 2017; Zou et al., 2018). The theoretical basis of SRI is similar to SPI proposed by McKee et al. (1993). SRI is defined as the unit standard normal deviate associated with the percentile of hydrologic runoff accumulated over a specific duration (Shukla & Wood, 2008). The first step is to fit a PDF to a given frequency distribution of data series for a gauging station. Akaike's Information Criterion (AIC), proposed by Akaike (1998), was used to evaluate the fitness of probability distribution, and the best fitted distribution was selected with the minimum AIC value (see Table S4). As shown in Figure 2, the Generalized Extreme Value (GEV) distribution with the minimum AIC value was chosen as the best fit for monthly streamflow in this study. The PDF parameters of GEV were then used to derive the cumulative probability of the observed monthly streamflow for a period of 15 years. The cumulative distribution function of the GEV distribution is given as follows (Hosking et al., 1985):

$$\mathrm{F(x)} = e^{-\left[1 - \mathcal{K}\left(\frac{x - \mu}{\alpha}\right)\right]^{\frac{1}{\mathcal{K}}}}, \tag{8}$$

where $\mathcal{K}$, α, and μ are shape, scale, and location parameters, respectively. The cumulative distribution of the monthly streamflow is then transformed into the standardized normal distribution with mean zero and variance one. The value of SRI can be obtained by calculating the SD for the magnitude of the observed streamflow deviating from a normally distributed random variable. A threshold of severity for SRI can be calculated based on the probability of exceeding an observed SRI value. Finally, the hydrological drought can be classified according to the threshold values of SRI. Based on the run theory (Nam et al., 2015; Yevjevich, 1969), drought events can be compared in terms of duration, severity, and intensity. The drought severity is defined as the total area of the SRI below a chosen threshold. The drought intensity can be calculated from dividing the drought severity by the duration.

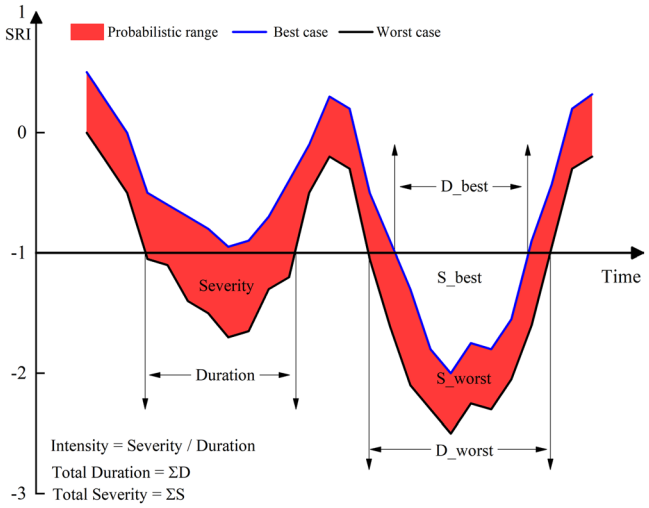

Figure 3. Schematic of probabilistic hydrological drought projections under best- and worst-case scenarios.

The probabilistic projection of hydrological droughts can be developed based on the SRI incorporating probabilistic hydrological predictions. In this study, a probabilistic distribution of SRI was generated by addressing both model structural and parameter uncertainties. A 95% confidence interval of SRI can then be obtained by calculating the 2.5th and 97.5th percentiles of the SRI distribution, leading to two hydrological drought scenarios including the worst-case scenario (the 2.5th percentile) and the best-case scenario (the 97.5th percentile). The SRI with the 95% confidence interval can be used to improve the reliability of drought risk assessment by characterizing uncertainties in hydrological drought prediction. As shown in Figure 3, the red curve band represents the probabilistic drought index where the blue curve indicates the drought evolution under the best-case scenario and the black curve indicates the drought evolution under the worst-case scenario. A hydrological drought event is identified when the SRI value is smaller than −1. The duration of the drought event is the period from the drought onset to termination. The accumulated SRI value below the threshold of −1 is defined as the severity of a drought event. To assess the multivariate characteristics of a single hydrological drought event, D_best and D_worst denote the duration of a drought event under the best- and worst-case scenarios, respectively. S_best and S_worst denote the severity of a drought event under the best- and worst-case scenarios, respectively. The intensity of the drought event can then be calculated through dividing the drought severity by its corresponding duration. Thus, I_best and I_worst denote the drought intensity under the best- and worst-case scenarios, respectively.

3. Results and Discussion

3.1. Validation of Convection-Permitting Climate Simulations

Figure 4 shows the comparison of spatial distributions of annual mean precipitation over Texas between the convection-permitting WRF simulation with the grid spacing of 4 km, the CFSR product with the grid spacing of 38 km, and the PRISM observation for the period from 1981 to 1995. As shown in Figures 4a–4c, there is a consistent spatial pattern of the annual mean precipitation for all the three data sets. The amount of precipitation is relatively low over West Texas and is increasing eastward gradually. According to the absolute (Figures 4d and 4e) and relative (Figures 4f and 4g) differences between different data sets (see Table S5 for the statistical assessment of significance of precipitation by the Wilcoxon's rank sum test), there is a significant dry bias in South Texas and a significant wet bias in North Texas between the WRF simulation and the PRISM observation, but there is no significant difference in Central-South Texas (Divisions 6–8). The study area is located in Central-South Texas (Divisions 6–8) near the mountainous and urban regions (San Antonio and Austin). The climate variables can be better simulated by the convection-permitting WRF model over complex terrains. As for the coarse-resolution CFSR product, there is a significant dry bias in North Texas and a significant wet bias in South Texas.

To better perform a quantitative comparison between WRF and CFSR, the region of Texas is divided into 10 climate divisions according to the U.S. National Climatic Data Center (NCDC), as shown in Figure 1. Figure 5 presents a quantitative assessment of model simulations using the Taylor diagram. The daily mean precipitation obtained from WRF has the COR between 0.6 and 0.9, the SD between 1 and 1.5, and the RMSE between 0.5 and 1. In comparison, the COR values of WRF are larger than those of the CFSR reanalysis, and the RMSE values of WRF are smaller than those of CFSR for all climate divisions. The larger the COR values and the smaller the RMSE values, the better the model performance. These results indicate that the convection-permitting WRF model has better performance in comparison with CFSR. This is because the spatial resolution (4 km) of the convection-permitting WRF model is high enough to explicitly resolve small-scale climate processes (convection processes) without the use of parameterization schemes, which are considered as the major source for model errors and uncertainties. Thus, the convection-permitting climate model is particularly useful for generating climate change information over complex terrains, such as watersheds, urban, or coastal regions. In addition, Table S6 shows the comparison of statistics used to evaluate precipitation simulation between WRF and PRISM as well as between CFSR and PRISM during 1981–

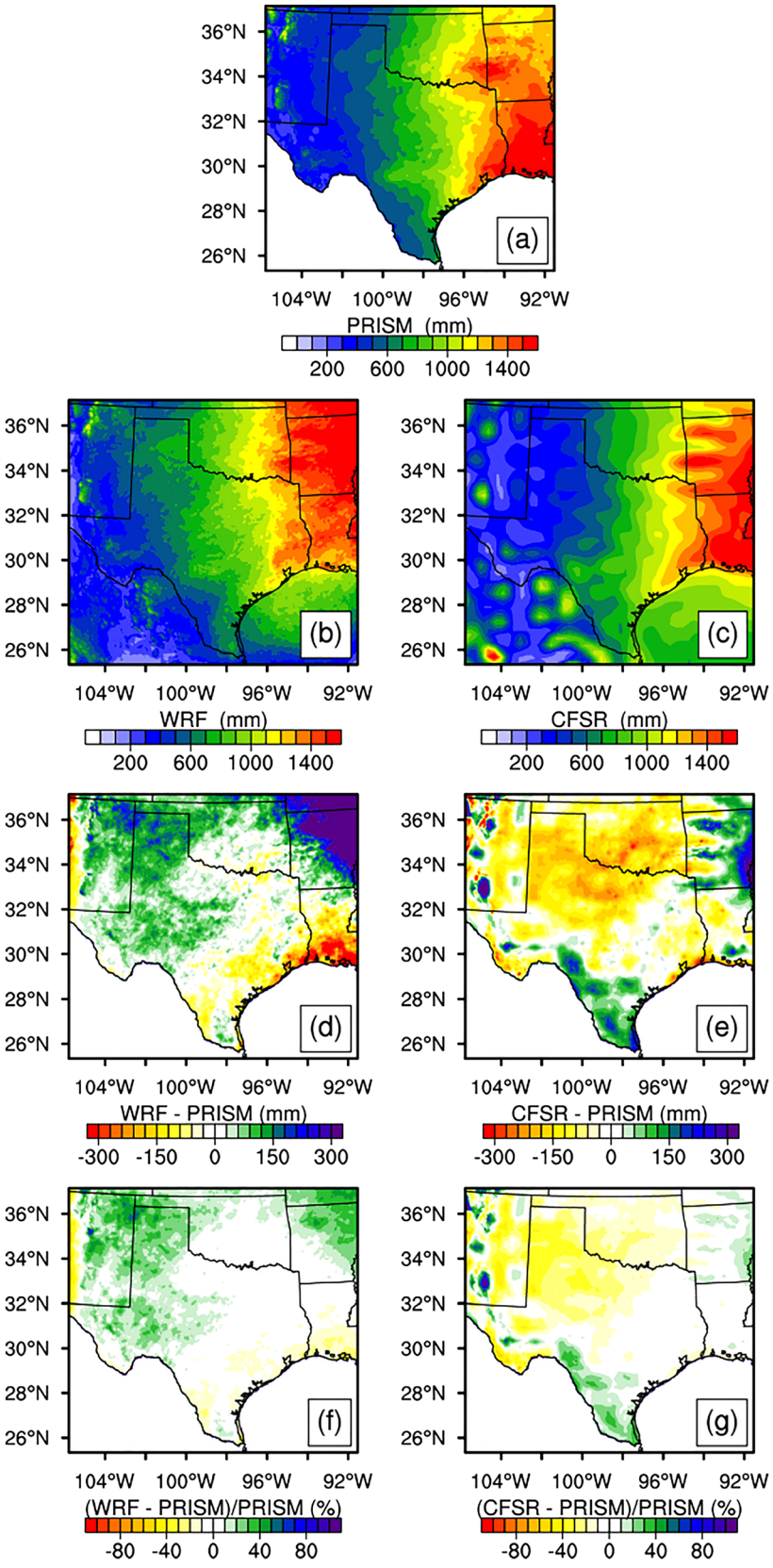

Figure 4. Comparison of spatial distributions of annual mean precipitation derived from the convection-permitting WRF simulation, the CFSR product, and the PRISM observation.

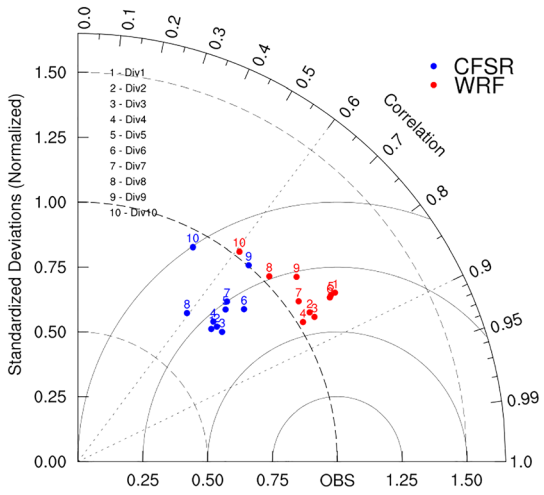

Figure 5. Comparison of model simulations of daily mean precipitation during 1981–1995 over 10 climate divisions of Texas.

1995. These indicate that the convection-permitting WRF model has better performance than CFSR due to the resulting larger SDs and CORs for all climate divisions of Texas.

Figure 6 depicts the comparison of spatial distributions of seasonal precipitation derived from the convection-permitting WRF simulation, the CFSR product, and the PRISM observation. According to the absolute differences between the WRF and the PRISM precipitation (WRF-PRISM) as well as those between the CFSR and the PRISM precipitation (CFSR-PRISM), it can be seen that both WRF and CFSR can adequately simulate the precipitation patterns over Texas for the winter months (DJF) in comparison with the PRISM observation. However, the WRF model overestimates the spring precipitation while CFSR tends to underestimate the spring precipitation over Texas. For summer (JJA) and fall (SON) seasons, the WRF model greatly improves the performance of precipitation simulation compared to CFSR, especially for South Texas, which is the focused region of this study. This is because the convective processes (e.g., precipitation and cloud processes) are more intense in spring and summer months, which can be explicitly resolved by the convection-permitting WRF model without the use of parameterization schemes (Prein et al., 2015). Table S7 shows the assessment of statistical significance on the differences of seasonal precipitation derived from WRF, PRISM, and CFSR (Figure 6) over 10 climate divisions of Texas.

The WRF model shows better performance in simulating annual and seasonal mean precipitation over Texas compared to the coarse-resolution CFSR. In fact, extreme precipitation and drought events are taking place frequently during wet seasons in Texas (Myoung & Nielsen-Gammon, 2010). It is thus necessary to conduct the convection-permitting climate simulation that can well capture spatial and temporal heterogeneities of precipitation in Texas. In addition, precipitation is the most important climate variable affecting hydrological processes at a basin scale (Liu et al., 2017). The accurate simulation of precipitation plays a crucial role in improving the reliability of hydrological prediction and drought assessment (Liu et al., 2017; Prein et al., 2015).

3.2. Validation of Hydrological Predictions and Reproduction of Drought Events

To assess hydrological drought characteristics, the WRF-simulated precipitation, temperature, and PET were used as forcing data to drive the hydrological models for generating streamflow time series for the two major river basins including GRB and BRB in South Texas. There is no significant difference between WRF-simulated precipitation and observed precipitation at the significance level of 5% for the two river basins (Table S5). In addition, the models were calibrated based on streamflow observations for a 10-year period from 1981–1990, and then the performance of the calibrated model was validated based on observations over the 5-year period from 1991–1995.

Figures 7 and 8 depict the comparison of the simulated and observed streamflow time series for the BRB and the GRB, respectively. As shown in Table S8, 84%, 95%, and 92% of observations in BRB are captured within the 95% uncertainty range of the simulated streamflow derived from HYMOD, SWAT, and HYMOD-SWAT, respectively. As for GRB, there are 88%, 79%, and 90% of observations captured within the 95% uncertainty range of the simulated streamflow derived from HYMOD, SWAT, and HYMOD-SWAT, respectively. Generally, the predictive performance by different hydrologic models is acceptable in terms of Nash-Sutcliffe efficiency (NSE), coefficient of determination (R^2), and the adjusted linear COR. In comparison, the HYMOD-SWAT model has relatively good performance for both river basins of Texas. This indicates that the coupled HYMOD-SWAT model performs superior than individual models and can thus be used to predict future streamflow regimes based on the projected climate information for the two major river basins.

SRI can be used to assess hydrological drought characteristics based on the predicted streamflow. Before assessing future hydrological droughts, it is necessary to examine the skill of SRI in reproducing historical drought events. Figure 9 depicts two severe drought events taking place during 1984–1985 and 1988–1990 based on the observed streamflow in two river basins. In the BRB, the severest drought events took place

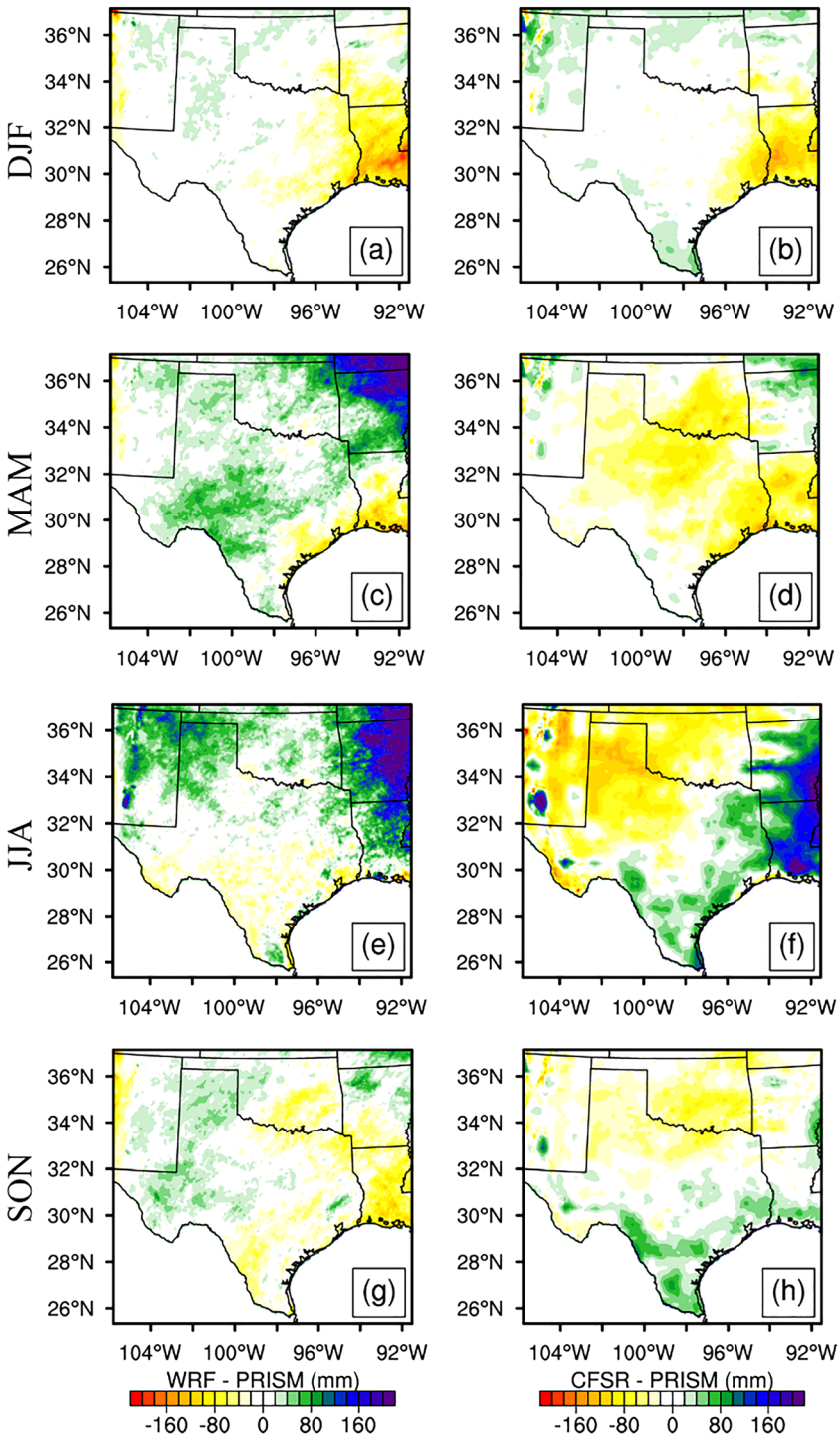

Figure 6. Comparison of spatial distributions of seasonal precipitation derived from the convection-permitting WRF simulation, the CFSR product, and the PRISM observation.

during the period from 1989 to 1990, which lasted for 8 months. In the GRB, the severest drought event occurred in 1984, which lasted for 9 months. These results are in good agreement with the drought report of Texas (Rosenzweig et al., 2001). The severest drought events hit Texas during the period from 1988 to 1990, which caused the largest economic loss on record in the United States. In addition, SRI captures the other seven severe hydrological drought events in South Texas from 1981 to 1995. SRI shows high skill in

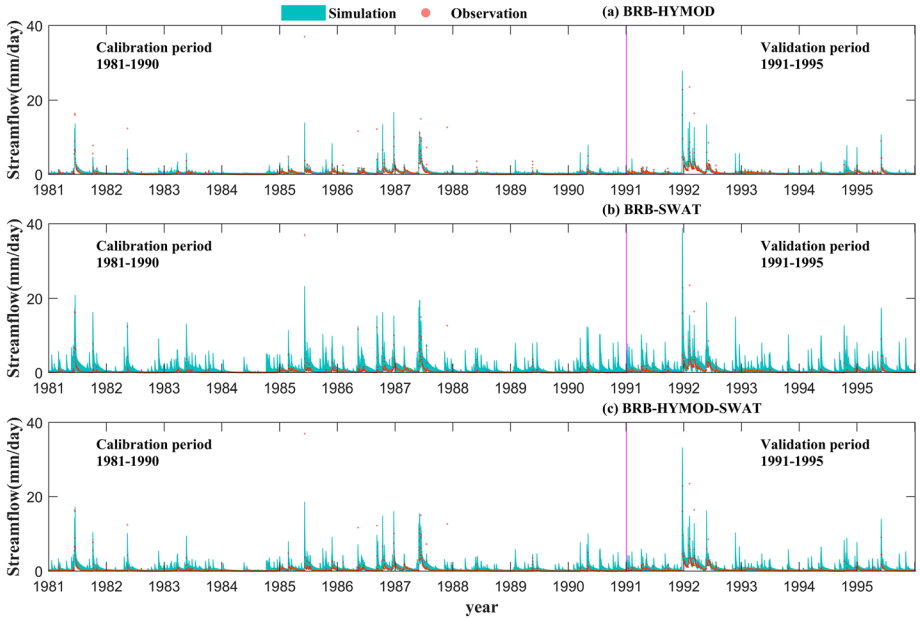

Figure 7. Comparison of observed (red point) and simulated (green bar) streamflow time series derived from (a) HYMOD, (b) SWAT, and (c) HYMOD-SWAT for the Blanco River Basin. The percentage of observations captured by the simulated uncertainty interval is (a) 84%, (b) 95%, and (c) 92%, respectively.

reproducing historical hydrological drought events and can thus be applied to assess the future hydrological drought episodes based on the predicted streamflow regimes.

Figure 9 shows the comparison between probabilistic hydrological droughts with a 95% uncertainty range and observations in the historical period (1981–1995). The best- and worst-case scenarios represent the 97.5th percentile and the 2.5th percentile of the derived SRI distribution, respectively. The pattern of probabilistic droughts agrees well with observations, which indicates that the probabilistic SRI can be used to

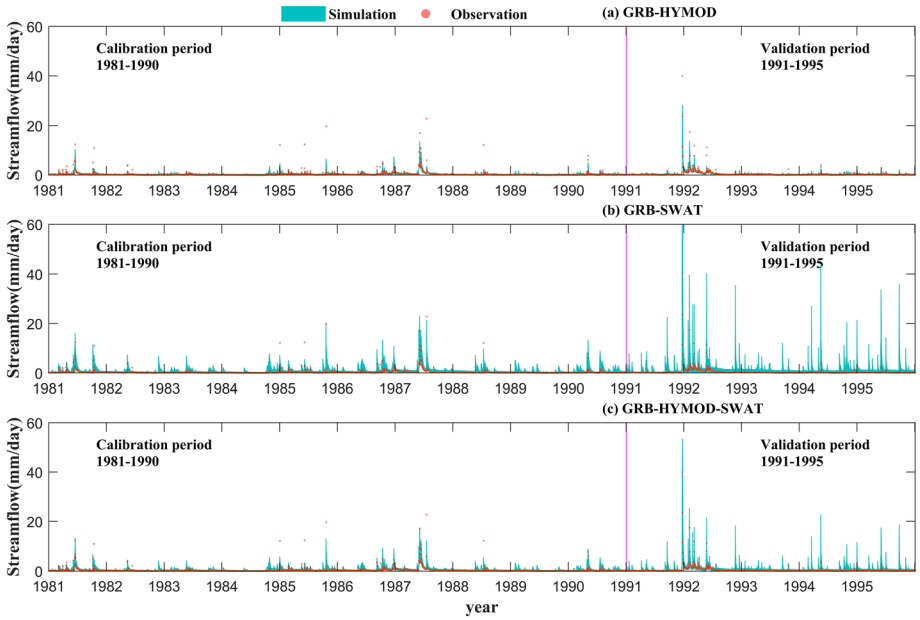

Figure 8. Comparison of observed (red point) and simulated (green bar) streamflow time series derived from (a) HYMOD, (b) SWAT, and (c) HYMOD-SWAT for the Guadalupe River Basin. The percentage of observations captured by the simulated uncertainty interval is (a) 88%, (b) 79%, and (c) 90%, respectively.

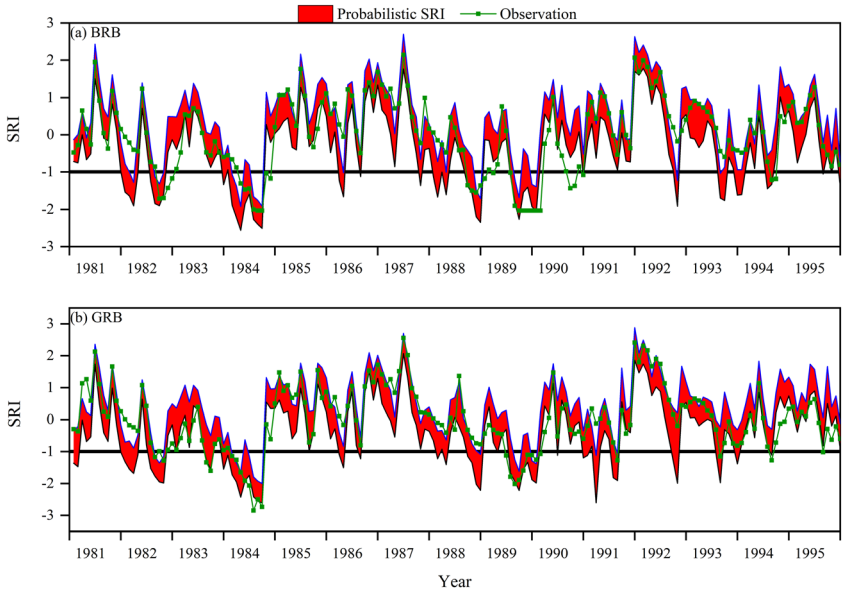

Figure 9. The time series of the SRI values derived for Guadalupe River Basin (GRB) and Blanco River Basin (BRB) under best- and worst-case scenarios in the historical period.

predict the long-term trend and the pattern of hydrological drought evolution. Quantitative assessment is also conduced to further examine the ability of the probabilistic SRI in reproducing historical drought events. In the worst-case scenario, 71% and 76% of observed droughts can be reproduced by the simulated SRI for GRB and BRB, respectively. Thus, the probabilistic SRI is capable of capturing the pattern and trend of historical hydrological droughts. This indicates that the probabilistic SRI has high skills of predicting the long-term trend and the pattern of hydrological drought evolution in a changing climate.

3.3. Probabilistic Assessment of Hydrological Drought Characteristics

To assess the future hydrological droughts, the time series of the SRI values can be estimated based on the daily streamflow forecast forced by the projected precipitation, and PET. Figures 10 and 11 present the time series of the projected monthly mean precipitation, PET, daily streamflow, and the derived SRI for two river basins in South Texas. The probabilistic forecast of daily streamflow with the 95% uncertainty range was produced to characterize uncertainties in model parameters and model structures (Figure 10b), leading to probabilistic hydrological drought assessment under best- and worst-case scenarios (Figure 10c).

As shown in Table S9, there are significant differences between historical and projected future precipitation, streamflow, and SRI for the two river basins (GRB and BRB) based on the Wilcoxon's rank sum test at the significance level of 5%. In addition, Figure 12 presents a comparison of the relative frequency between historical and future daily precipitation in two major river basins. The frequencies of light and moderate precipitation with the amount smaller than 25 mm are projected to decline, whereas the frequency of heavy precipitation with the amount larger than 25 mm is projected to increase in the future. Results imply that precipitation extremes are expected to increase by the end of this century, whereas the drying trend can be attributed to a considerable decrease in light and moderate precipitation. These are in agreement with the previous findings (Prein et al., 2016; Villarini et al., 2011; G. Wang, Wang, et al., 2017; Westra et al., 2014).

The statistics of future hydrological drought characteristics including the frequency, duration, and severity and intensity under best- and worst-case scenarios are provided in Table S10. For the GRB, a total of eight drought events can be detected for the period from 2085 to 2099 under the best-case scenario. The longest duration (D_best) of drought events is 2 months, and the highest intensity (I_best) is −1.39. By contrast, a total of 23 drought events can be expected under the worst-case scenario. The longest duration and the highest intensity of drought events are projected to be 10 months and −1.50, respectively. As for BRB, a total of five future droughts are detected under the best-case scenario, with the longest duration (D_best) of 2 months and the highest intensity (I_best) of −1.35. In contrast, a total of 22 drought events are projected under the

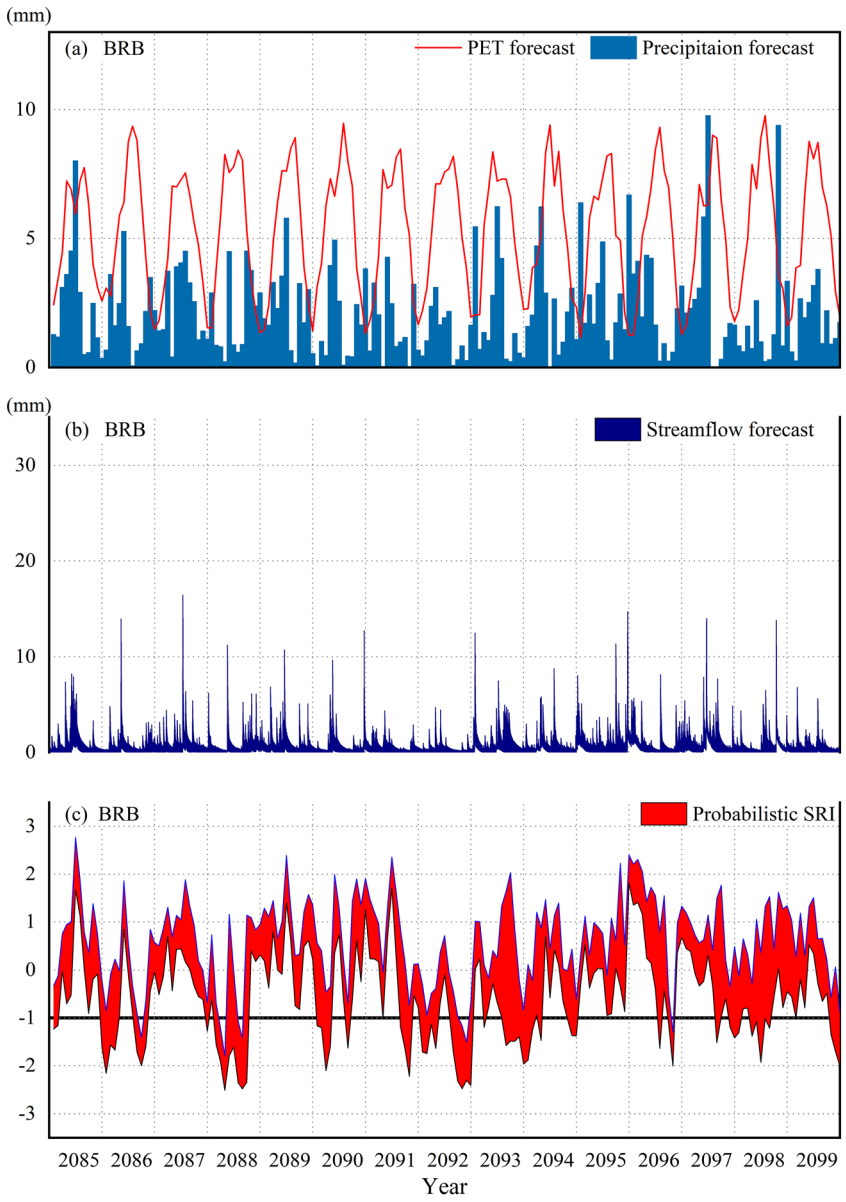

Figure 10. The time series of the projected monthly mean precipitation, PET, daily streamflow, and the derived SRI with the 95% uncertainty range for the Blanco River Basin (BRB).

worst-case scenario, with the longest duration of 8 months and the highest intensity of −1.51. This indicates that the total duration and intensity of projected hydrological droughts will increase under the worst-case scenario compared to those under the best-case scenario, which provides meaningful insights into the potential risks of drought assessment. It is thus necessary to conduct probabilistic hydrological drought projections by characterizing different sources of uncertainty in order to reduce potential risks of losses and damages caused by droughts.

3.4. Projected Changes in Hydrological Drought Characteristics

To assess climate change impacts on hydrological droughts, historical and future SRI values are compared against each other. As shown in Table S10, under the worst-case scenario, the number of hydrological drought events is projected to double by the end of this century for two river basins. The total duration of droughts is projected to become longer, and the severity and intensity of droughts are projected to increase.

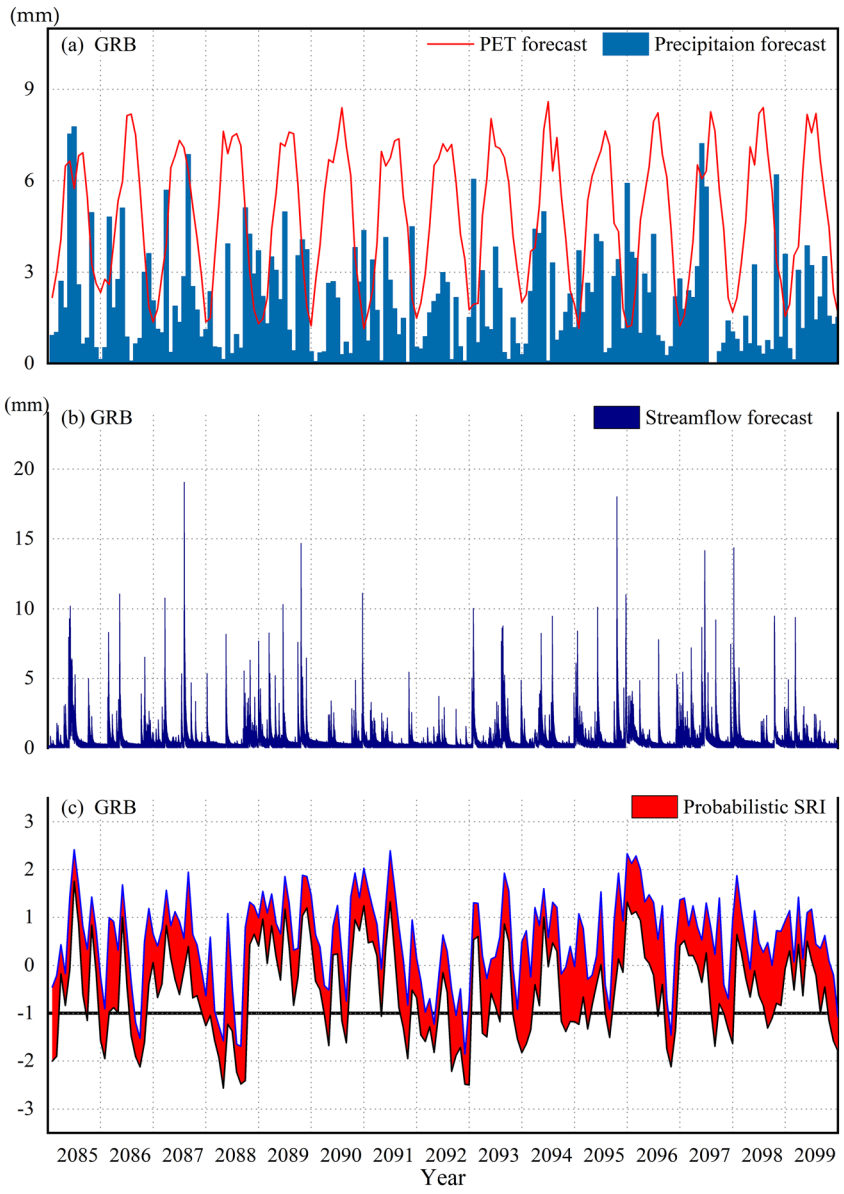

Figure 11. The time series of the projected monthly mean precipitation, PET, daily streamflow, and the derived SRI with the 95% uncertainty range for the Guadalupe River Basin (GRB).

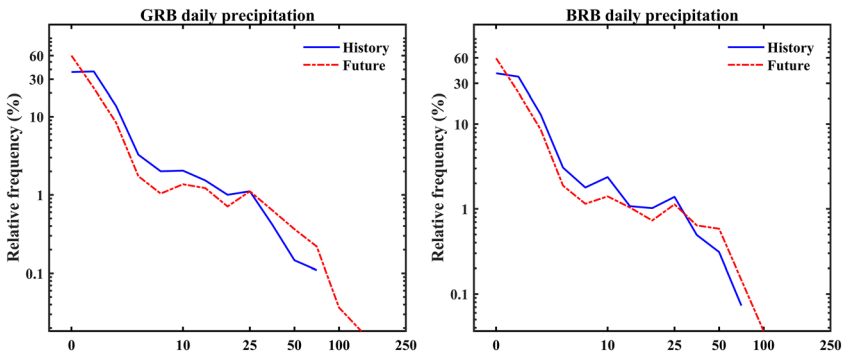

Figure 12. Comparison of the relative frequency between historical and future daily precipitation in Guadalupe River Basin (GRB) and Blanco River Basin (BRB).

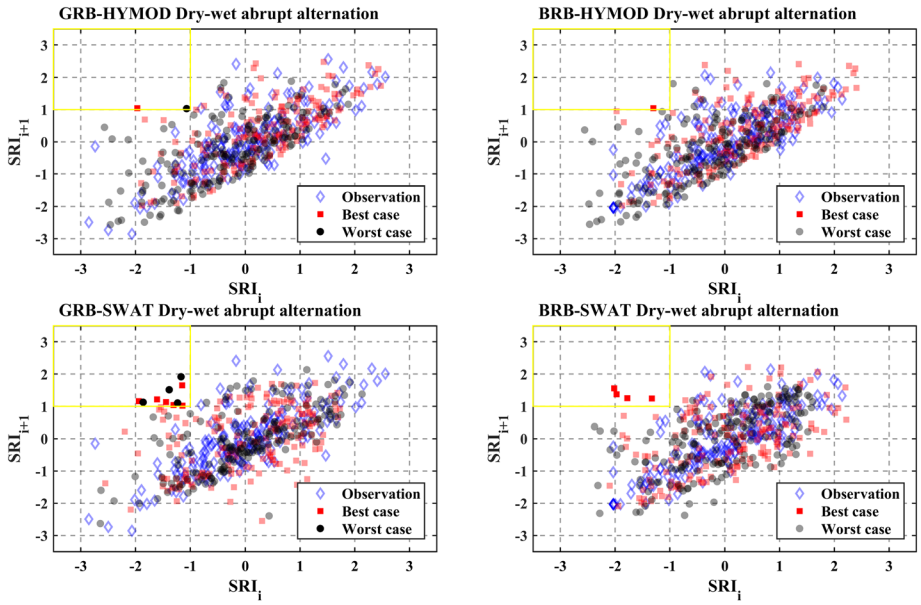

Figure 13. The SRI values used to assess historical and future DWAA events under best- and worst-case scenarios based on HYMOD and SWAT model simulations. The SRI with a value larger than 1 indicates a wet condition, and the SRI with a value smaller than −1 represents a dry condition. The points located in the yellow rectangle of the upper-left corner represent the DWAA events in which a dry condition occurs in *i*th month (SRI_i is smaller than −1) and abruptly turns into a wet condition in the next month (SRI_{i+1} is larger than 1).

Our findings reveal that the extreme precipitation can abruptly alter the drought condition from dry to wet for a short period of time. This phenomenon is a dry-wet abrupt alternation (DWAA). The SRI was used in this study to evaluate the dry and wet conditions of hydrological regimes. SRI_i with a value smaller than −1 represents a dry condition, and SRI_i with a value larger than 1 indicates a wet condition in *i*th month. If the SRI_{i+1} value is larger than 1 (or smaller than −1) in $i+1$st month and the SRI_i value is smaller than −1 (or larger than 1) in *i*th month, this indicates a DWAA event. As highlighted by the yellow rectangles in Figure 13, the number of DWAA events is projected to increase in a changing climate under the best-case scenario, whereas no historical record of such an extreme event is found in the two river basins for both HYMOD and SWAT model simulations. As for the GRB, there will be a larger increase in the number of DWAA events under the best-case scenario in comparison with the worst-case scenario. As for the BRB, no DWAA event is projected under the worst-case scenario. Therefore, the DWAA event is projected to become more frequent under the best-case scenario rather than the worst-case scenario. It should be noted that when a dry-wet alternation event is found under the best-case scenario, it may not be detected simultaneously under the worst-case scenario due to the uncertainties arising from model structures and parameters (as shown in Figure S1). The DWAA is a new feature and trend of drought anomalies, which can greatly damage the soil structure and have great potential for causing flash floods and soil erosion.

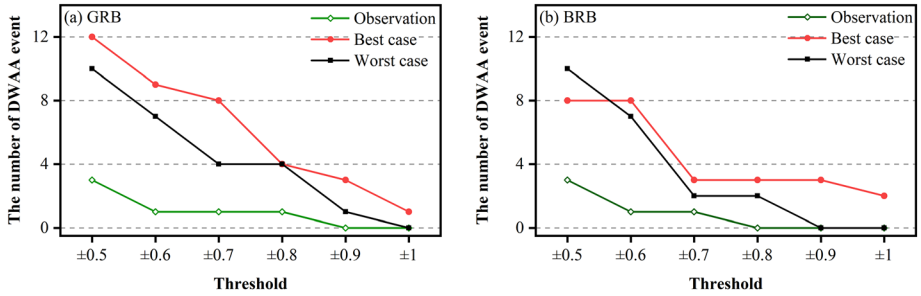

Figure 14. The relationship between different thresholds of dry/wet conditions and the number of DWAA events in the two river basins. The threshold of dry-wet alternation (e.g., ±0.5) indicates the dry condition is SRI smaller than −0.5, and the wet condition is SRI larger than 0.5.

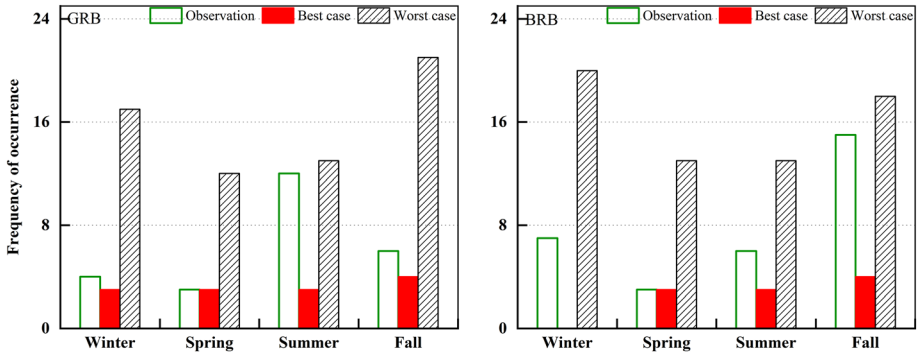

Figure 15. Frequency of occurrence of historical and future hydrological droughts across four seasons for Guadalupe River Basin (GRB) and Blanco River Basin (BRB).

Moreover, the DWAA can cause a substantial increase in natural disasters such as landslides and mud-rock flows in mountainous areas.

A sensitivity analysis of thresholds used to identify the DWAA event was also performed to conduct a robust and comprehensive assessment of such extreme events. Previous studies identified the dry-wet transition by a threshold of smaller than −0.5 (Hao et al., 2017; Wu & Chen, 2019; Z. Zhang et al., 2018), which can lead to a large number of dry-wet transition events. However, the threshold of smaller than −0.5 does not indicate a severe drought. Figure 14 presents the relationship between the threshold of dry/wet conditions and the number of DWAA events. The increasing number of detected DWAA events attributes to a smaller threshold of dry/wet condition. Moreover, the number of DWAA events is projected to increase under the best-case scenario for all thresholds of dry/wet conditions. Compared to the worst-case scenario, the number of DWAA events is expected to increase under the best-case scenario. When the threshold is larger than 0.6 (SRI ≤ -0.6 indicates a dry condition and SRI ≥ 0.6 indicates a wet condition), the number of DWAA events in the best-case scenario is larger than the number of DWAA events in the worst-case scenario. Moreover, the number of DWAA events in the worst-case scenario is larger than the number of DWAA in the historical period. These findings indicate that the DWAA is expected to become more severe and frequent under the best-case scenario (97.5th of the SRI distribution represents a wetter scenario) under climate change.

Figure 15 shows the frequency of occurrence of historical and future hydrological droughts across four seasons for GRB and BRB, respectively. It can be seen that the historical hydrological droughts occurred most frequently in summer for GRB, and the frequency of future hydrological droughts is projected to become higher in fall. The seasonal hydrological droughts are expected to experience a temporal shift from summer to fall for the GRB by the end of the 21st century. As for BRB, the seasonal pattern of future hydrological droughts is experiencing a temporal shift from fall to winter. These reveal different seasonal changes in future hydrological drought patterns for two river basins in a changing climate.

It should be noted that although both model parameter and structural uncertainties were addressed in this study, the other sources of uncertainty (e.g., RCP climate scenarios and forcing data) should also be taken into account in future studies to further improve the accuracy of hydrological drought projection. In addition, the long-term convection-permitting climate simulation (more than 30 years) is desired to enable a comprehensive assessment of droughts across different time scales when the computational resources become available.

4. Conclusions

In this study, we develop probabilistic projections of hydrological drought characteristics through a convection-permitting climate simulation and a multimodel hydrologic prediction for two major river basins in South Texas of the United States. The WRF model with the horizontal grid spacing of 4 km shows high skill in simulating the spatial and temporal variability of precipitation, which is the most important climate variable for assessing all types of droughts. Moreover, the convection-permitting WRF simulation can well represent the spatial heterogeneity of watershed characteristics, which plays a crucial role in assessing hydrologic responses to droughts. In addition, both model parameter and structural uncertainties

inherent in streamflow prediction are addressed explicitly, leading to the probabilistic projection of hydrological droughts under best- and worst-case scenarios. The proposed probabilistic hydrological drought projection improves the reliability and robustness of drought risk assessment, which is useful for policymakers and stakeholders to develop sound strategies for drought preparedness and mitigation planning in a changing climate.

The probabilistic hydrological drought projection depicts the future evolution of spatiotemporal characteristics of droughts under the best- and worst-case scenarios that represent the 97.5th percentile and the 2.5th percentile of the SRI distribution, respectively. The probabilistic projection of SRI reflects the complexity in hydrological drought assessment due to various sources of uncertainty. By contrast, the worst-case scenario of drought assessment provides meaningful insights into the potential risk of assessing drought evolution characteristics. It is thus necessary to develop probabilistic hydrological drought projections by characterizing different sources of uncertainty in order to improve the reliability of assessing future changes in drought characteristics under climate change. As the evolution of drought characteristics varies under best- and worst-case scenarios, optimistic and conservative alternatives can be provided to decision makers who may choose the appropriate one based on their risk attitudes.

The prolonged droughts are expected to be punctuated by the increasing extreme precipitation events, leading to an increasing number of the DWAA events that can cause flash floods and soil erosion. A high frequency of hydrological drought events is also projected for the fall season by the end of this century, especially for the GRB where hydrological droughts are projected to experience a temporal shift from summer to fall. And hydrological droughts are also expected to experience a temporal shift from fall to winter in the Blanco river basin. These findings not only advance our understanding of future changes in seasonal characteristics of hydrological droughts but also provide meaningful insights into agricultural development and water resources planning for Texas under climate change.

Data Availability Statement

In this study, the PRISM data set was produced by the PRISM Climate Group at Oregon State University, and the CFSR product was provided by the NCEP. The daily hydrological data were collected from the U. S. MOPEX data set. The climate outputs from 15 CMIP5 GCMs (Table S1) were collected to generate the perturbed ensemble mean signal. All the hydroclimatic data files can be accessed online (at https://data.mendeley.com/datasets/ydv2d2cmfp/2).

Acknowledgments

This research was supported by the National Natural Science Foundation of China (Grant No. 51809223) and the Hong Kong Polytechnic University Start-up Grant (Grant No. 1-ZE8S). We would also like to express our sincere gratitude to the editor and three anonymous reviewers for their constructive comments and suggestions.

References

Abbaspour, K., Rouholahnejad, E., Vaghefi, S., Srinivasan, R., Yang, H., & Kløve, B. (2015). A continental-scale hydrology and water quality model for Europe: Calibration and uncertainty of a high-resolution large-scale SWAT model. *Journal of Hydrology*, *524*, 733–752. https://doi.org/10.1016/j.jhydrol.2015.03.027

Abera, W., Formetta, G., Brocca, L., & Rigon, R. (2017). Modeling the water budget of the Upper Blue Nile basin using the JGrass-NewAge model system and satellite data. *Hydrology and Earth System Sciences*, *21*(6), 3145–3165. https://doi.org/10.5194/hess-21-3145-2017

Akaike, H. (1998). Information theory and an extension of the maximum likelihood principle. In *Selected papers of Hirotugu Akaike*, edited (pp. 199–213). New York, NY: Springer.

Allen, R., Pereira, L., Raes, D., & Smith, M. (1998). *Crop vapotranspiration: Guidelines for computing crop water requirements*, *Irrigation and drainage paper 56*. Rome, Italy: Food and Agriculture Organization of the United Nations.

Andrieu, C., & Thoms, J. (2008). A tutorial on adaptive MCMC. *Statistics and Computing*, *18*(4), 343–373. https://doi.org/10.1007/s11222-008-9110-y

Carvalho, K. S., & Wang, S. (2019). Characterizing the Indian Ocean sea level changes and potential coastal flooding impacts under global warming. *Journal of Hydrology*, *569*, 373–386. https://doi.org/10.1016/j.jhydrol.2018.11.072

Chen, H., Wang, S., & Wang, Y. (2020). Exploring abrupt alternations between wet and dry conditions on the basis of historical observations and convection-permitting climate model simulations. *Journal of Geophysical Research: Atmospheres*, *125*, e2019JD031982. https://doi.org/10.1029/2019JD031982

Daly, C., Halbleib, M., Smith, J. I., Gibson, W. P., Doggett, M. K., Taylor, G. H., et al. (2008). Physiographically sensitive mapping of climatological temperature and precipitation across the conterminous United States. *International Journal of Climatology*, *28*(15), 2031–2064. https://doi.org/10.1002/joc.1688

Dehghani, M., Saghafian, B., Saleh, F. N., Farokhnia, A., & Noori, R. (2014). Uncertainty analysis of streamflow drought forecast using artificial neural networks and Monte-Carlo simulation. *International Journal of Climatology*, *34*(4), 1169–1180. https://doi.org/10.1002/joc.3754

Deser, C., Knutti, R., Solomon, S., & Phillips, A. S. (2012). Communication of the role of natural variability in future North American climate. *Nature Climate Change*, *2*(11), 775–779. https://doi.org/10.1038/nclimate1562

Duan, Q., Schaake, J., Andreassian, V., Franks, S., Goteti, G., Gupta, H., et al. (2006). Model parameter estimation experiment (MOPEX): An overview of science strategy and major results from the second and third workshops. *Journal of Hydrology*, *320*(1–2), 3–17. https://doi.org/10.1016/j.jhydrol.2005.07.031

Gassman, P., Reyes, M., Green, C., & Arnold, J. (2007). The soil and water assessment tool: Historical development, applications, and future research directions. *Transactions of the ASABE*, *50*(4), 1211–1250. https://doi.org/10.13031/2013.23637

Gelman, A., & Rubin, D. B. (1992). Inference from iterative simulation using multiple sequences. *Statistical Science*, *7*(4), 457–472. https://doi.org/10.1214/ss/1177011136

Hao, Z., Hao, F., Singh, V. P., & Ouyang, W. (2017). Quantitative risk assessment of the effects of drought on extreme temperature in eastern China. *Journal of Geophysical Research: Atmospheres*, *122*, 9050–9059. https://doi.org/10.1002/2017JD027030

Herman, J., Reed, P., & Wagener, T. (2013). Time-varying sensitivity analysis clarifies the effects of watershed model formulation on model behavior. *Water Resources Research*, *49*, 1400–1414. https://doi.org/10.1002/wrcr.20124

Hong, S., & Pan, H. (1996). Nonlocal boundary layer vertical diffusion in a medium-range forecast model. *Monthly Weather Review*, *124*(10), 2322–2339. https://doi.org/10.1175/1520-0493(1996)124<2322:NBLVDI>2.0.CO;2

Hosking, J. R. M., Wallis, J. R., & Wood, E. F. (1985). Estimation of the generalized extreme-value distribution by the method of probability-weighted moments. *Technometrics*, *27*(3), 251–261. https://doi.org/10.1080/00401706.1985.10488049

Iacono, M. J., Delamere, J. S., Mlawer, E. J., Shephard, M. W., Clough, S. A., & Collins, W. D. (2008). Radiative forcing by long-lived greenhouse gases: Calculations with the AER radiative transfer models. *Journal of Geophysical Research*, *113*, D13103. https://doi.org/10.1029/2008JD009944

Jiménez, P. A., Dudhia, J., González-Rouco, J. F., Navarro, J., Montávez, J. P., & García-Bustamante, E. (2012). A revised scheme for the WRF surface layer formulation. *Monthly Weather Review*, *140*(3), 898–918. https://doi.org/10.1175/MWR-D-11-00056.1

Karl, T. R. (1986). The sensitivity of the Palmer Drought Severity Index and Palmer's Z-index to their calibration coefficients including potential evapotranspiration. *Journal of Climate and Applied Meteorology*, *25*(1), 77–86. https://doi.org/10.1175/1520-0450(1986)025<0077:TSOTPD>2.0.CO;2

Kendon, E. J., Ban, N., Roberts, N. M., Fowler, H. J., Roberts, M. J., Chan, S. C., et al. (2017). Do convection-permitting regional climate models improve projections of future precipitation change? *Bulletin of the American Meteorological Society*, *98*(1), 79–93. https://doi.org/10.1175/BAMS-D-15-0004.1

Li, K., Huang, G., & Wang, S. (2019). Market-based stochastic optimization of water resources systems for improving drought resilience and economic efficiency in arid regions. *Journal of Cleaner Production*, *233*, 522–537. https://doi.org/10.1016/j.jclepro.2019.05.379

Liu, C., Ikeda, K., Rasmussen, R., Barlage, M., Newman, A. J., Prein, A. F., et al. (2017). Continental-scale convection-permitting modeling of the current and future climate of North America. *Climate Dynamics*, *49*(1–2), 71–95. https://doi.org/10.1007/s00382-016-3327-9

Liu, C., Ikeda, K., Thompson, G., Rasmussen, R., & Dudhia, J. (2011). High-resolution simulations of wintertime precipitation in the Colorado headwaters region: Sensitivity to physics parameterizations. *Monthly Weather Review*, *139*(11), 3533–3553. https://doi.org/10.1175/MWR-D-11-00009.1

Liu, L., Hong, Y., Bednarczyk, C. N., Yong, B., Shafer, M. A., Riley, R., & Hocker, J. E. (2012). Hydro-climatological drought analyses and projections using meteorological and hydrological drought indices: A case study in Blue River basin, Oklahoma. *Water Resources Management*, *26*(10), 2761–2779. https://doi.org/10.1007/s11269-012-0044-y

McKee, T. B., Doesken, N. J., & Kleist, J. (1993). The relationship of drought frequency and duration to time scales. In *Proceedings of the 8th Conference on Applied Climatology* (pp. 179–184). Boston, MA: American Meteorological Society.

Metropolis, N., Rosenbluth, A. W., Rosenbluth, M. N., Teller, A. H., & Teller, E. (1953). Equation of state calculations by fast computing machines. *The Journal of Chemical Physics*, *21*(6), 1087–1092. https://doi.org/10.1063/1.1699114

Mishra, A. K., & Singh, V. P. (2010). A review of drought concepts. *Journal of Hydrology*, *19*(NA), 333–349. https://doi.org/10.1139/a11-013

Modarres, R. (2007). Streamflow drought time series forecasting. *Stochastic Environmental Research and Risk Assessment*, *21*(3), 223–233. https://doi.org/10.1007/s00477-006-0058-1

Moore, R. (1985). The probability-distributed principle and runoff production at point and basin scales. *Hydrological Sciences Journal*, *30*(2), 273–297. https://doi.org/10.1080/02626668509490989

Myoung, B., & Nielsen-Gammon, J. W. (2010). The convective instability pathway to warm season drought in Texas. Part I: The role of convective inhibition and its modulation by soil moisture. *Journal of Climate*, *23*(17), 4461–4473. https://doi.org/10.1175/2010JCLI2946.1

Nalbantis, I., & Tsakiris, G. (2009). Assessment of hydrological drought revisited. *Water Resources Management*, *23*(5), 881–897. https://doi.org/10.1007/s11269-008-9305-1

Nam, W.-H., Hayes, M. J., Svoboda, M. D., Tadesse, T., & Wilhite, D. A. (2015). Drought hazard assessment in the context of climate change for South Korea. *Agricultural Water Management*, *160*, 106–117. https://doi.org/10.1016/j.agwat.2015.06.029

Naumann, G., Alfieri, L., Wyser, K., Mentaschi, L., Betts, R. A., Carrao, H., et al. (2018). Global changes in drought conditions under different levels of warming. *Geophysical Research Letters*, *45*, 3285–3296. https://doi.org/10.1002/2017GL076521

Neitsch, S., Arnold, J., Kiniry, J., & Williams, J. (2011). Soil and water assessment tool theoretical documentation version 2009, *Texas Water Resources Institute*.

Niu, G. Y., Yang, Z. L., Mitchell, K. E., Chen, F., Ek, M. B., Barlage, M., et al. (2011). The community Noah land surface model with multiparameterization options (Noah-MP): 1. Model description and evaluation with local-scale measurements. *Journal of Geophysical Research*, *116*, D12109. https://doi.org/10.1029/2010JD015139

Oguntunde, P. G., Abiodun, B. J., & Lischeid, G. (2017). Impacts of climate change on hydro-meteorological drought over the Volta basin, West Africa. *Global and Planetary Change*, *155*, 121–132. https://doi.org/10.1016/j.gloplacha.2017.07.003

Oguntunde, P. G., Lischeid, G., & Abiodun, B. J. (2018). Impacts of climate variability and change on drought characteristics in the Niger River basin, West Africa. *Stochastic Environmental Research and Risk Assessment*, *32*(4), 1017–1034. https://doi.org/10.1007/s00477-017-1484-y

Pereira, V. R., Blain, G. C., de Avila, A. M. H., Pires, R. C. D., & Pintos, H. S. (2018). Impacts of climate change on drought: Changes to drier conditions at the beginning of the crop growing season in Southern Brazil. *Bragantia*, *77*(1), 201–211. https://doi.org/10.1590/1678-4499.2017007

Prein, A. F., Langhans, W., Fosser, G., Ferrone, A., Ban, N., Goergen, K., et al. (2015). A review on regional convection-permitting climate modeling: Demonstrations, prospects, and challenges. *Reviews of Geophysics*, *53*, 323–361. https://doi.org/10.1002/2014RG000475

Prein, A. F., Rasmussen, R. M., Ikeda, K., Liu, C., Clark, M. P., & Holland, G. J. (2016). The future intensification of hourly precipitation extremes. *Nature Climate Change*, *7*(1), 48–52. https://doi.org/10.1038/nclimate3168

Rasmussen, K. L., Prein, A. F., Rasmussen, R. M., Ikeda, K., & Liu, C. (2017). Changes in the convective population and thermodynamic environments in convection-permitting regional climate simulations over the United States. *Climate Dynamics*, *55*(1-2), 383–408. https://doi.org/10.1007/s00382-017-4000-7

Rodrigues, D., Gupta, H., Mendiondo, E., & Oliveira, P. (2015). Assessing uncertainties in surface water security: An empirical multimodel approach. *Water Resources Research*, *51*, 9013–9028. https://doi.org/10.1002/2014WR016691

Rosenzweig, C., Iglesias, A., Yang, X., Epstein, P. R., & Chivian, E. (2001). Climate change and extreme weather events—Implications for food production, plant diseases, and pests. *Global Change & Human Health*, *2*(2), 90–104. https://doi.org/10.1023/A:1015086831467

Roy, T., Gupta, H. V., Serrat-Capdevila, A., & Valdes, J. B. (2017). Using satellite-based evapotranspiration estimates to improve the structure of a simple conceptual rainfall-runoff model. *Hydrology and Earth System Sciences*, *21*(2), 879–896. https://doi.org/10.5194/hess-21-879-2017

Sadegh, M., Ragno, E., & AghaKouchak, A. (2017). Multivariate copula analysis toolbox (MvCAT): Describing dependence and underlying uncertainty using a Bayesian framework. *Water Resources Research*, *53*, 5166–5183. https://doi.org/10.1002/2016WR020242

Samaniego, L., Kumar, R., & Zink, M. (2013). Implications of parameter uncertainty on soil moisture drought analysis in Germany. *Journal of Hydrometeorology*, *14*(1), 47–68. https://doi.org/10.1175/JHM-D-12-075.1

Schlaepfer, D. R., Bradford, J. B., Lauenroth, W. K., Munson, S. M., Tietjen, B., Hall, S. A., et al. (2017). Climate change reduces extent of temperate drylands and intensifies drought in deep soils. *Nature Communications*, *8*, 14196. https://doi.org/10.1038/ncomms14196

Shafer, B. (1982). Development of a surface water supply index (SWSI) to assess the severity of drought conditions in snowpack runoff areas. In *Proceedings of the 50th Annual Western Snow Conference* (pp. 164–175). Fort Collins: Colorado State University.

Shukla, S., & Wood, A. W. (2008). Use of a standardized runoff index for characterizing hydrologic drought. *Geophysical Research Letters*, *35*, L02405. https://doi.org/10.1029/2007GL032487

Silverman, N. L., Maneta, M. P., Chen, S. H., & Harper, J. T. (2013). Dynamically downscaled winter precipitation over complex terrain of the central Rockies of Western Montana, USA. *Water Resources Research*, *49*, 458–470. https://doi.org/10.1029/2012WR012874

Sorooshian, S., & Dracup, J. A. (1980). Stochastic parameter estimation procedures for hydrologie rainfall-runoff models: Correlated and heteroscedastic error cases. *Water Resources Research*, *16*(2), 430–442. https://doi.org/10.1029/WR016i002p00430

Tabari, H., Nikbakht, J., & Talaee, P. H. (2013). Hydrological drought assessment in Northwestern Iran based on streamflow drought index (SDI). *Water Resources Management*, *27*(1), 137–151. https://doi.org/10.1007/s11269-012-0173-3

Thompson, G., Field, P. R., Rasmussen, R. M., & Hall, W. D. (2008). Explicit forecasts of winter precipitation using an improved bulk microphysics scheme. Part II: Implementation of a new snow parameterization. *Monthly Weather Review*, *136*(12), 5095–5115. https://doi.org/10.1175/2008MWR2387.1

Tsakiris, G., Pangalou, D., & Vangelis, H. (2007). Regional drought assessment based on the reconnaissance drought index (RDI). *Water Resources Management*, *21*(5), 821–833. https://doi.org/10.1007/s11269-006-9105-4

Vicente-Serrano, S. M., López-Moreno, J. I., Beguería, S., Lorenzo-Lacruz, J., Azorin-Molina, C., & Morán-Tejeda, E. (2011). Accurate computation of a streamflow drought index. *Journal of Hydrologic Engineering*, *17*(2), 318–332. https://doi.org/10.1061/(ASCE)HE.1943-5584.0000433

Villarini, G., Smith, J. A., Baeck, M. L., Vitolo, R., Stephenson, D. B., & Krajewski, W. F. (2011). On the frequency of heavy rainfall for the Midwest of the United States. *Journal of Hydrology*, *400*(1-2), 103–120. https://doi.org/10.1016/j.jhydrol.2011.01.027

Vrugt, J. A. (2016). Markov chain Monte Carlo simulation using the DREAM software package: Theory, concepts, and MATLAB implementation. *Environmental Modelling & Software*, *75*, 273–316. https://doi.org/10.1016/j.envsoft.2015.08.013

Vrugt, J. A., Ter Braak, C. J., Clark, M. P., Hyman, J. M., & Robinson, B. A. (2008). Treatment of input uncertainty in hydrologic modeling: Doing hydrology backward with Markov chain Monte Carlo simulation. *Water Resources Research*, *44*, W00B09. https://doi.org/10.1029/2007WR006720

Vu, M. T., Vo, N. D., Gourbesville, P., Raghavan, S. V., & Liong, S. Y. (2017). Hydro-meteorological drought assessment under climate change impact over the Vu Gia-Thu Bon River basin, Vietnam. *Hydrological Sciences Journal-Journal Des Sciences Hydrologiques*, *62*(10), 1654–1668. https://doi.org/10.1080/02626667.2017.1346374

Wakazuki, Y., & Rasmussen, R. (2015). Incremental dynamical downscaling for probabilistic analysis based on multiple GCM projections. *Geophysical Research Letters*, *42*, 10,847–10,855. https://doi.org/10.1002/2015GL066242

Wang, G., Wang, D., Trenberth, K. E., Erfanian, A., Yu, M., Bosilovich, M. G., & Parr, D. T. (2017). The peak structure and future changes of the relationships between extreme precipitation and temperature. *Nature Climate Change*, *7*(4), 268–274. https://doi.org/10.1038/nclimate3239

Wang, S., Ancell, B., Huang, G., & Baetz, B. (2018). Improving robustness of hydrologic ensemble predictions through probabilistic pre-and post-processing in sequential data assimilation. *Water Resources Research*, *54*, 2129–2151. https://doi.org/10.1002/2018WR022546

Wang, S., Huang, G., Baetz, B., & Ancell, B. (2017). Towards robust quantification and reduction of uncertainty in hydrologic predictions: Integration of particle Markov chain Monte Carlo and factorial polynomial chaos expansion. *Journal of Hydrology*, *548*, 484–497. https://doi.org/10.1016/j.jhydrol.2017.03.027

Wang, S., & Wang, Y. (2019). Improving probabilistic hydroclimatic projections through high-resolution convection-permitting climate modeling and Markov chain Monte Carlo simulations. *Climate Dynamics*, *53*(3-4), 1613–1636. https://doi.org/10.1007/s00382-019-04702-7

Wang, Y., Geerts, B., & Liu, C. (2018). A 30-year convection-permitting regional climate simulation over the interior Western United States. Part I: Validation. *International Journal of Climatology*, *38*(9), 3684–3704. https://doi.org/10.1002/joc.5527

Wang, Z. L., Zhong, R. D., Lai, C. G., Zeng, Z. Y., Lian, Y. Q., & Bai, X. Y. (2018). Climate change enhances the severity and variability of drought in the Pearl River basin in South China in the 21st century. *Agricultural and Forest Meteorology*, *249*, 149–162. https://doi.org/10.1016/j.agrformet.2017.12.077

Westra, S., Fowler, H., Evans, J., Alexander, L., Berg, P., Johnson, F., et al. (2014). Future changes to the intensity and frequency of short-duration extreme rainfall. *Reviews of Geophysics*, *52*, 522–555. https://doi.org/10.1002/2014RG000464

Wilby, R. L., & Harris, I. (2006). A framework for assessing uncertainties in climate change impacts: Low-flow scenarios for the River Thames, UK. *Water Resources Research*, *42*, W02419. https://doi.org/10.1029/2005WR004065

Wu, J., & Chen, X. (2019). Spatiotemporal trends of dryness/wetness duration and severity: The respective contribution of precipitation and temperature. *Atmospheric Research*, *216*, 176–185. https://doi.org/10.1016/j.atmosres.2018.10.005

Yang, Z. L., Niu, G. Y., Mitchell, K. E., Chen, F., Ek, M. B., Barlage, M., et al. (2011). The community Noah land surface model with multiparameterization options (Noah-MP): 2. Evaluation over global river basins. *Journal of Geophysical Research*, *116*, D12110. https://doi.org/10.1029/2010JD015140

Yevjevich, V. M. (1969). An objective approach to definitions and investigations of continental hydrologic droughts. *Journal of Hydrology*, *7*(3), 353–353. https://doi.org/10.1016/0022-1694(69)90110-3

Yu, P. S., Yang, T. C., Kuo, C. M., Tseng, H. W., & Chen, S. T. (2015). Climate change impacts on streamflow drought: A case study in Tseng-Wen Reservoir Catchment in Southern Taiwan. *Climate*, *3*(1), 42–62. https://doi.org/10.3390/cli3010042

Yuan, Z., Xu, J. J., Chen, J., Huo, J. J., Yu, Y. Y., Locher, P., & Xu, B. (2017). Drought assessment and projection under climate change: A case study in the Middle and Lower Jinsha River basin. *Advances in Meteorology*, *2017*, 1–16. http://doi.org/10.1155/2017/5757238

Zargar, A., Sadiq, R., Naser, B., & Khan, F. I. (2011). A review of drought indices. *Environmental Reviews*, *19*(NA), 333–349. https://doi.org/10.1016/j.jhydrol.2010.07.012

Zhang, B., Wang, S., & Wang, Y. (2019). Copula-based convection-permitting projections of future changes in multivariate drought characteristics. *Journal of Geophysical Research: Atmospheres*, *124*, 7460–7483. https://doi.org/10.1029/2019JD030686

Zhang, Q., & Zhang, J. Q. (2016). Drought hazard assessment in typical corn cultivated areas of China at present and potential climate change. *Natural Hazards*, *81*(2), 1323–1331. https://doi.org/10.1007/s11069-015-2137-4

Zhang, Z., Li, Y., Chen, F., Barlage, M., & Li, Z. (2018). Evaluation of convection-permitting WRF CONUS simulation on the relationship between soil moisture and heatwaves. *Climate Dynamics*, *55*(1-2), 235–252. https://doi.org/10.1007/s00382-018-4508-5

Zhu, J., Wang, S., & Huang, G. (2019). Assessing climate change impacts on human-perceived temperature extremes and underlying uncertainties. *Journal of Geophysical Research: Atmospheres*, *124*, 3800–3821. https://doi.org/10.1029/2018JD029444

Zotarelli, L., Dukes, M. D., Romero, C. C., Migliaccio, K. W., & Morgan, K. T. (2010). Step by step calculation of the Penman-Monteith Evapotranspiration (FAO-56 Method), *Institute of Food and Agricultural Sciences. University of Florida*.

Zou, L., Xia, J., & She, D. X. (2018). Analysis of impacts of climate change and human activities on hydrological drought: A case study in the Wei River basin, China. *Water Resources Management*, *32*(4), 1421–1438. https://doi.org/10.1007/s11269-017-1877-1